Terrestrial Evaporation and Moisture Drainage in a Warmer Climate

Daniel J. Short Gianotti[1], Ruzbeh Akbar[1], Andrew F. Feldman[1], Guido D. Salvucci[2], and Dara Entekhabi[1]

[1]Parsons Laboratory, Department of Civil and Environmental Engineering, Massachusetts Institute of Technology.

[2]Department of Earth and Environment, Boston University.

Corresponding author: Daniel Short Gianotti (gianotti@mit.edu)

Key Points:

- Assess sensitivity of terrestrial evaporation and drainage to climate perturbations based on satellite-era soil moisture observations
- Climate perturbation effects are superposable despite nonlinear flux mechanisms and mixed-sign effects of each climate perturbation
- Changes in water fluxes poorly-captured by hydroclimate indices (Budyko framework) with changing precipitation extremes

Abstract

To determine hydrologic changes in a warmer climate, we impose precipitation and potential evaporation (E_o) perturbations on hydrologic response functions constructed from precipitation and satellite soil moisture observations across the United States. Despite nonlinearities in the evaporation (E) and drainage (D) responses and opposing-sign perturbations, changes in individual fluxes are superposable. Empirical frameworks (Budyko) can misrepresent changes in E/D partitioning by neglecting shifts/trends in hydrologic regime and subseasonal precipitation dynamics. E/D both increase to balance mean precipitation ($\bar{P}$) increases, and increased E_o reduces soil moisture. E and D are generally more elastic to changes in $\bar{P}$ than E_o. The results suggest that (1) the impacts of regional hydrologic perturbations may allow for simple superposition/scaling, (2) changes in timing/intensity of precipitation may have substantial impacts on mean moisture states and fluxes, and (3) changes to the distribution of surface moisture states are likely more relevant for E/D partitioning than common aridity indices.

Plain Language Summary

We use satellite observations of soil moisture and expected increase in air temperature to determine how evaporation and soil drainage (to groundwater recharge and rivers/streamflow) will change in a warmer climate. The impacts of drier air, more rainfall, and more extreme rainfall (drier dry days and wetter wet days) can largely be considered separately and then added, which will help when predicting a specific location's water balance using scenarios from global climate models. In typical scenarios, soils are likely to dry, evaporation is likely to increase, and — when precipitation increases — drainage to groundwater/streams is likely to increase as well. Evaporation and drainage are relatively more sensitive to changes in precipitation and humidity in the Western US than the East, and the Corn Belt is particularly susceptible to changes in precipitation intensity. Common methods of determining changes in evaporation and drainage which neglect changes in soil moisture may have large errors in global change scenarios.

Introduction

Our best predictions for the future of the terrestrial water cycle come from Global Climate and Earth System Models (GCMs, ESMs), which forecast general increases in precipitation (Greve et

al., 2018; O'Gorman et al., 2012; O'Gorman & Schneider, 2008) and atmospheric water demand (Q. Fu & Feng, 2014), along with distributional changes in precipitation intensity (Greve et al., 2014; Hirabayashi et al., 2013; Schewe et al., 2014). The spatial patterns of these changes are driven by the coupling between radiative processes, cloud physics, and moisture advection, and are affected to a large degree by unpredictable internal variability in global atmospheric dynamics (Anderson et al., 2015; Greve et al., 2018; Greve & Seneviratne, 2015; Hawkins & Sutton, 2011; Samset et al., 2016). The modeled land-surface response to these changes is represented through parameterizations — as simple as single functions or as complex as a land-surface biosphere model — and is rarely separated from the uncertain atmospheric drivers or confronted with observations (Berg et al., 2017).

Water cycle changes are often summarized as changes in an aridity index — typically the ratio of mean precipitation (P) to mean potential evaporation (E_o) — following well-known hydro-climatological frameworks which suggest that this ratio is sufficient (under some assumptions) to determine land-surface water flux partitioning into evaporation and drainage/runoff (Budyko, 1963; Oldekop, 1911; Roderick & Farquhar, 2011; Turc, 1954). Changes in both E_o and mean precipitation may offset each other, potentially with no change in $\bar{E}/E_o$. Projected changes in storm characteristics, such as intensification of precipitation extremes (Kharin et al., 2013; O'Gorman & Schneider, 2009), are neglected in these frameworks.

Land surface moisture fluxes are state dependent, however (Akbar et al., 2018; Haghighi et al., 2018; Koster et al., 2018; Short Gianotti et al., 2019). Thus, changes in flux partitioning are better understood through (1) changes in the probability distribution of soil moisture (θ, the surface moisture state variable, highly inconsistent across models; Koster et al., 2009) and (2) its downstream impacts on evaporation (E), surface runoff (R), and drainage/percolation (D). E determines surface temperatures and humidity through the surface energy balance. D and R together determine streamflow and groundwater recharge, and will be assessed together in this study as D (see discussion below). Both outfluxes, E and D, depend nonlinearly on θ. It is thus necessary to query observations of the land surface to see which changes in atmospheric forcings are expected to add linearly and which may be offsetting.

Observations of surface soil moisture (Entekhabi et al., 2010; O'Neill et al., 2016) and inferred surface moisture fluxes (Akbar et al., 2019) provide an opportunity to constrain these downstream variables. The use of historical observations to develop hydrologic response functions does not replace ESMs which couple the synchronous dynamics of atmospheric circulation, surface hydrology, and land-atmosphere feedbacks (Berg et al., 2016; Milly & Dunne, 2016; Swann, 2018). These observations instead provide a framework to assess the response of each component of the surface water balance to different climate perturbations free from model-imposed parameterizations. Additionally, daily time series allow finer temporal assessment of θ variations and the mechanisms of E/D partitioning, an advantage over use of historical annual means in other frameworks (Berghuijs et al., 2017; Greve et al., 2018; Roderick et al., 2014; Roderick & Farquhar, 2011).

This motivates our research question: How will precipitation be partitioned into evaporation and subsurface drainage fluxes in a warmer climate with changes in potential evaporation (E_o), mean precipitation ($\bar{P}$), and precipitation extremes?

To address this question, we use an observation-driven framework to assess how key fluxes pull the landscape water balance in opposing directions in response to climate perturbations. We use hydrologic response functions estimated from historical precipitation and satellite soil moisture observations to (a) determine evaporative and drainage responses to precipitation forcing and soil moisture state. We then (b) use the retrieved E and D response functions to determine changes in warm-season fluxes across the Contiguous United States (ConUS) subject to perturbed (i) E_o, (ii) $\bar{P}$, (iii) precipitation extremes, and (iv) coincident changes in all three.

As we will find, these perturbations lend themselves well to superposition and magnitude-scaling, and so the choice of perturbation magnitudes is not particularly significant, except in relation to the magnitude of impact on E or D.

We will compare the results to typical aridity-index (Budyko) methods for estimating changes in E and D and find that changes to the precipitation distribution/extremes are critical in E/D partitioning. Finally we calculate elasticities of E and D to changes in E_o, $\bar{P}$, and precipitation extremes.

Methods

Water balance model and parameter estimation

To derive time series of surface soil moisture, evaporation, and drainage we follow the method of Akbar et al., (2019). Surface soil moisture for the summers (May-September) of 2015-2017 is modeled using an estimation approach with two objective functions to minimize squared differences between modeled surface microwave brightness temperatures and observations from the SMAP satellite (Entekhabi et al., 2010; O'Neill et al., 2016) while additionally conserving water mass. The problem is solved with an adjoint variational method where the water balance equation is incorporated using a Lagrange multiplier. The water balance is driven by gridded gauge-based precipitation observations from NCEP's Climate Prediction Center (Chen et al., 2008) and determines effluxes of water from the homogeneous surface layer as

$$\Delta z \cdot \frac{d\theta}{dt} = P(t) - E(\theta) - D(\theta) \quad \#(1)$$

where Δz is the thickness of the surface layer, θ is the volumetric soil moisture (modeled as uniform within the layer), $P(t)$ is the precipitation rate, $E(\theta)$ is evapotranspiration to the atmosphere, and $D(\theta)$ is drainage losses to subsurface soil layers. Four parameters — E_o, b, c, and d determine the shapes of the evaporation (E) and drainage (D) components:

$$E(\theta; E_o, b) = \frac{1}{2} \cdot \left(1 + \tanh\left[8\left(\frac{\theta}{\phi} - \frac{1}{1+e^{-b}} + 0.25\right)\right]\right) \cdot E_o \quad \#(2)$$

$$D(\theta; c, d) = c \cdot \left(\frac{\theta}{\phi}\right)^{d} \quad \#(3)$$

for porosity ϕ. The parameters Δz, E_o, b, c, and d are estimated in Akbar et al. (2019) for each 36km SMAP pixel and create a forward water model for surface soil moisture given precipitation inputs and the previous soil moisture state. The loss functions (2) and (3) are intentionally flexible enough to span most plausible moisture/flux relations: b shifts the evaporation function as a function of soil moisture, c and d are effective Clapp-Hornberger parameters (Clapp & Hornberger, 1978). The estimated Δz determines the thickness of the surface layer that maintains hydrologic mass balance. An example loss function is shown for a location in Southern Iowa in Figure 1a.

Climate Perturbations

To begin we impose warm-season (MJJAS) climate perturbations as 3%, 6%, 9%, and 12% increases of E_o, 2.5%, 5%, 7.5%, and 10% increases in $\bar{P}$, and 2.5%, 5%, 7.5%, and 10% increases in "heavy" (upper decile) precipitation, denoted P_{X90}. The values are selected as typical of the modeled global mean (including oceans) response to 1-4°C increases in global temperature (Fläschner et al., 2016; Hartmann et al., 2013; Kharin et al., 2013; Lambert & Webb, 2008; McVicar et al., 2012; Pall et al., 2007; Pendergrass et al., 2017; Samset et al., 2016; Scheff & Frierson, 2014), but this selection is somewhat arbitrary. We assert that these perturbations are not intended to represent real forecasts of future climate. Forecasts of perturbations at local scale will depend on uncertain changes in atmospheric water vapor dynamics (Anderson et al., 2015; Byrne & O'Gorman, 2015; Dai et al., 2018; Gianotti et al., 2014; Muller et al., 2011; Prein & Pendergrass, 2019; Romps, 2011; Sohn & Park, 2010; Thackeray et al., 2018; Vecchi et al., 2006) and land-atmosphere-biosphere feedbacks (Greve et al., 2018; Greve & Seneviratne, 2015; Novick et al., 2016; Rigden et al., 2018), and must be estimated in fully-coupled settings (Berg et al., 2016; Berg & Sheffield, 2018; Milly & Dunne, 2016; Swann, 2018). Results from this study can then be applied to variable fields of perturbations.

To investigate water demand-only effects, the E_o parameter is perturbed at each location. E values from Equation 2 represent the soil moisture-conditioned mean-state evaporation, and hence E_o represents the mean-state potential evaporation. E itself varies at the timestep of our model (sub-daily), as it is driven by daily precipitation influxes and soil moisture states. See Figure 1b for loss function impacts.

In all scenarios, precipitation occurrence is unchanged, as is the timing of the ranked precipitation intensity (if the July 12th rain event is the 10th heaviest observed amount at a given location, this timing/ranking will remain true in all scenarios). The intensities themselves are altered by either: (a) increasing mean precipitation or (b) through an amplification of extreme events. To increase mean precipitation, intensities on all wet days are multiplied by a scaling factor $1 + m \cdot v$, using $v = 0.025$, $m = \{1,2,3,4\}$ (Figure 1c). Amplification of extreme precipitation re-allocates some precipitation from the dry tail of the intensity distribution to the wet tail in a manner which leaves both the mean and maximum precipitation unchanged (Figure 1d and Supplementary Figure 1). See Supplementary Information for further details. Note that this re-allocation has no impact on E/D partitioning in the Budyko framework.

Water Balance

The time series of θ, E, and D are determined by integrating the water balance (1) using the CPC precipitation observations at 3-minute time steps and the parameters estimated in Akbar et al. (2019) (additionally, see Akbar et al., (2019) for validation of θ against SMAP Level 3 soil moisture retrievals, D against gauged streamflow, and E against flux tower latent heat flux measurements). Explicit Hortonian overland runoff is generated when precipitation influx exceeds the storage capacity of the entire pixel, but is rare at 36km scale using 3-minute time steps. Drainage from the surface layer drives both groundwater recharge and surface streamflow in this framework; the two are not estimated separately. Seasonal mean Hortonian runoff out of the saturated pixel is $< 0.01\%$ of seasonal mean precipitation for all locations. Adding this runoff to estimated drainage fluxes has no impact on the results.

We integrate the water balance (1) using the observations (Figure 1a), the altered potential evaporation parameter (E_o experiment — Figure 1b), the altered precipitation through scaling ($\bar{P}$ experiment — Figure 1c), and the altered precipitation through amplification of extremes (P_{X90} experiment — Figure 1d) independently to determine perturbative effects on evaporation and drainage partitioning. An example of each experiment is shown for a single summer in Figure 1. We also integrate the water balance with all interacting effects (Combined experiment) for analysis. In each case, the dynamics by which the probability distribution of soil moisture plays

179 out through the moisture-dependent flux functions determine the aggregate flux partitioning into
180 E and D.

181 **Results**

182 As found previously (Akbar et al., 2019), warm season continental evaporation under present
183 conditions is generally larger than drainage by a factor of 2 or more (Figure 2a). As shown in
184 Figure 1b, increasing E_o shifts the PDF of soil moisture towards drier states, decreasing the D
185 component faster than the E component. E increases (and D decreases) by roughly 0.05-0.1
186 mm/day for a 3% increase in E_o in the wettest regions (Figure 2b), with notable changes in the
187 Eastern ConUS, and minimal changes in the already water-limited West.

188 Increasing water supply through increased precipitation ($\bar{P}$ experiment; Figure 2c) leads to
189 increases in both E and D as expected, with larger magnitude increases in D in wetter, more
190 energy-limited regions and larger magnitude increases in E in drier, more water-limited regions
191 (effectively defined by the typical 100th parallel arid/humid division of ConUS hydroclimate).
192 Drainage is essentially unchanged in arid regions, where existing E_o dominates surface fluxes.
193 The shift in the soil moisture marginal distribution does not significantly increase drainage in
194 these arid regions since the drainage function (steep only for wetter soils) is largely insensitive to
195 soil moisture under drier conditions (see Fig. 1a).

196 The redistribution of precipitation from light rainfall days to heavy days (P_{X90} experiment;
197 Figure 2d) leads to near-universal increases in D at the expense of E. This is perhaps expected
198 due to the sensitivity of hydraulic conductivity to soil moisture, but not *a priori* certain due to the
199 complex interplay of precipitation regimes, climatic conditions, and soil texture controls on
200 evaporative and drainage fluxes. The dominant impacts in the Eastern US highlight the role the
201 wet end of the precipitation and soil moisture distributions can play in seasonal-scale water
202 budgets, effectively offsetting E_o (atmospheric demand) changes in 2b with no change to the
203 seasonal supply.

204 When integrating the water balance using the combined forcings of the E_o, $\bar{P}$, and P_{X90}
205 experiments, we find near-universal increases in both mean E and D across the range of changes
206 to E_o and precipitation (Figure 2e). As with the subcomponents shown in 2b-d, D is primarily

207 impacted in the Eastern ConUS, while E has more-nearly-equivalent magnitude changes across
208 climate gradients for equivalent boundary condition perturbations. Recall that water supply
209 changes in these experiments are driven by equivalent *relative* changes, e.g., 5% of local mean
210 precipitation, rather than absolute changes in mm/day. Mean soil moisture decreases universally
211 across the ConUS as well for the combined experiment (Supplementary Figure 2), which is also
212 projected in coupled model experiments (Gu et al., 2019). The largest magnitude decreases occur
213 in the Ohio and Mississippi River Valleys, effectively shifting the arid/humid transition zone to
214 the East.

215 On average across the ConUS, a 3% increase in E_o alone (spatial average of leftmost column of
216 Figure 2b) increases E by a little more than 3 mm over a single warm season (0.017 mm/day or
217 1% of the ConUS-averaged E). A 2.5% increase in mean precipitation increases E by a little
218 more than 5 mm, and a 2.5% increase in the upper decile of precipitation (transferred from the
219 driest days) decreases E by 2.6 mm. The combined effect is an average 5.6 mm, 1.5% of the
220 ConUS average, and equivalent to a roughly 0.82 W/m^2 latent heat equivalent. These are all
221 roughly an order of magnitude larger than the corresponding (same sign) changes in surface soil
222 moisture storage.

223 *Water balance sensitivities to climate perturbations using superposition*

224 In Figure 2 — while each location is driven by the unique local characteristics of the retrieved
225 moisture loss functions — all locations are subject to identical relative perturbations, which
226 would not be the case in a broader future climate change scenario. We investigate the impact of
227 the relative perturbation magnitudes on the combined (Figure 2e) experiment in Supplementary
228 Figures 3-5 and find similar spatial patterns with changes in E/D partitioning magnitudes.
229 Exploring every combination of E_o, $\bar{P}$, and P_{X90} perturbations is infeasible, and it prompts the
230 question of how significant the interactions of multiple simultaneous perturbations is on changes
231 to E/D partitioning.

232 We find that adding the change in evaporation ΔE (or changes in drainage ΔD) from each of the
233 E_o, $\bar{P}$, and P_{X90} perturbations modeled independently is quite similar to the ΔE from imposing
234 the perturbations separately. Figure 3a shows the difference between the rightmost column of
235 Figure 2e ($E_o + 12\%$, $\bar{P} + 10\%$, and $P_{X90} + 10\%$, all perturbations simultaneously) and the sum

of the rightmost columns of Figure 2b-d. Errors are on the order of 1% or less, suggesting counterintuitively small impact of interactions between moisture supply and demand when averaged over the warm season.

We also find that scaling the impact of a perturbation is a close approximation of the impact of a scaled perturbation. Figure 3b shows the error in estimating ΔE in the rightmost column of Figure 2e ($E_o + 12\%$, $\bar{P} + 10\%$, and $P_{X90} + 10\%$ simultaneously) as four times ΔE in the leftmost column ($E_o + 3\%$, $\bar{P} + 2.5\%$, and $P_{X90} + 2.5\%$ simultaneously). Just as for superposition errors (combining different types of perturbations), combining multiple, say, 3% perturbations of E_o to get a 12% E_o perturbation works quite well. Errors are on the order of 2% or less in terms of ΔE, and much less in terms of the total $E + \Delta E$ estimate for the season.

Comparison with aridity-index approach: The Budyko framework misses important dynamics

The integration of the water balance in (1)-(3) results in time series of E across the ConUS, which can then be used to fit the spatially-varying n parameter of the standard hydroclimatological Budyko curve (Choudhury, 1999) for each pixel location:

$$\frac{E}{E_o} = \frac{P}{(P^n + E_o^n)^{\frac{1}{n}}} \#(4)$$

Without the actual evaporation (E) time series, n is typically either assumed constant (often $n = 2$ as from Turc [1954], although for a single continent-wide fit we find better fit with $n = 2.24$), or n comes somewhat circularly from land surface model output, where the internal functions driving water flux partitioning are themselves parameterized. We emphasize that using model output to fit these hydroclimatological parameters without some ingested water cycle data will necessarily return results based largely on the parameters used to drive the same land surface model. We fit n for each pixel using monthly aggregated values across the warm season using total least-squares (or "errors in variables") regression (Figure 4a), giving a spatial map of the n parameter (Figure 4b). This n estimation technique is independent of these circularities arising from use of land surface model outputs.

Changes in evaporation (ΔE) due to perturbations of E_o and $\bar{P}$ alone are similar for the framework in this study and the Budyko-based method (Figure 4c, $r^2 = 0.88$ for $E_o + 12\%$, $r^2 = 0.96$ for $\bar{P} + 10\%$, similar for ΔD and for smaller perturbations), but with some bias. Errors between the methods are nearly entirely explained by changes in surface moisture storage, and the Budyko method's evaporation bias for increased $\bar{P}$ is similarly due to neglecting the shift in mean soil moisture towards wetter, more drainage-favorable conditions.

Changes in the distribution of precipitation intensities, however, have no representation in the Budyko framework (Figure 4c $\Delta P_{X90} + 10\%$), and can be a major player in the partitioning of E and D (bias in ΔE by a factor of 2, and $r^2 = 0.58$ for all effects combined).

Elasticity of evaporation and drainage to $\boldsymbol{E_o}$, $\boldsymbol{\bar{P}}$, *and extreme* $\boldsymbol{P}$ *perturbations*

To assess relative impacts with more spatial granularity, we calculate the rate of change of each hydrologic response to a given climate perturbation (Supplementary Figure 6). When normalized, these are elasticities of fluxes to perturbations (Andréassian et al., 2016; Chiew, 2006; G. Fu et al., 2007; Risbey & Entekhabi, 1996; Sankarasubramanian et al., 2001; Yang & Yang, 2011). These elasticities are calculated as regression slopes of E versus E_o (normalized by observed E/E_o) for 0-12% changes in E_o, of E vs $\bar{P}$ (normalized by observed $E/\bar{P}$) for 0-10% changes in $\bar{P}$, and of E vs P_{X90} (normalized by observed E/P_{X90}) for 0-10% changes in P_{X90} — where P_{X90} is the amount of precipitation in the upper decile of the observed precipitation distribution. P_{X90} increasing by 5% represents the wettest days originally providing 10% of seasonal average precipitation now provide 10.5% of seasonal precipitation, and the driest days contributing 0.5% of seasonal precipitation now see no rain. Elasticities for drainage are calculated similarly.

Evaporation is more sensitive to relative changes in $\bar{P}$ than E_o (both positive elasticities) in 74% of ConUS pixels, and drainage is more sensitive to relative changes in $\bar{P}$ than E_o in 99% of pixels. Differences between these numbers are due to the difference in effect of surface soil drying/wetting for E and D (i.e., transient climate change effects of changes in storage). The general finding that a 1% change in moisture supply $\bar{P}$ has a larger impact on downstream fluxes

than a 1% change in moisture demand E_o is typical of elasticity studies using aridity index frameworks and modeled evaporation data (Berghuijs et al., 2017).

Drainage elasticities to change in mean potential evaporation E_o and mean precipitation $\bar{P}$ are an order of magnitude larger than for E, and with opposing signs (Supplementary Figures 6d and 6e). The shifts in precipitation extremes P_{X90} has equivalent magnitude as shifts in $\bar{P}$, amplifying the impacts on drainage.

Separating the ConUS into East and West halves (Supplementary Figure 7) leads to average E increases of 0.17 mm/day per each additional 1 mm/day of E_o in the East (aggregate elasticity of 0.34) versus 0.05 mm/day in the West (aggregate elasticity of 0.28). East (West) ConUS E increases by 0.35 (0.66) mm/day per 1 mm/day of additional $\bar{P}$, an aggregate elasticity of 0.48 (0.72). By changing precipitation extremes, E in the East (West) decreases 0.62 (0.34) mm seasonally per 1 mm of precipitation reallocated to wet days from dry days, an aggregate elasticity of -0.30 (-0.14). Actual evaporation increases slightly with increased extremes in the most arid pixels (Supplementary Figures 6 and 10) due to a shift of the soil moisture PDF from "Stage III" evaporation to "Stage II" evaporation, but magnitudes of both fluxes are vanishingly small.

Discussion and Conclusions

This study assesses the responses of evaporation and soil drainage to changes in potential evaporation, mean precipitation, and the distribution of daily precipitation intensities using a water balance framework developing observed fields of surface soil brightness temperatures and precipitation alone. These response sensitivities have been previously calculated using models, but we argue that modeled sensitivities are inherently determined by land surface parameterizations of evapotranspiration and soil moisture pedotransfer functions. This study confronts these sensitivities with data directly—in an "offline" mode with no representation of feedbacks (e.g., canopy conductance) other than that captured in the water cycle observations—and thus serves as a partial derivative of land surface moisture fluxes to climate perturbations, holding feedbacks constant. We claim that this uncoupled (but data-driven) approach serves as a necessary counterbalance to data-blind models (but with fully coupled dynamics), and we

advocate for future assimilation and reanalysis schemes incorporating dynamical land surface and vegetation data streams.

We find that the E/D partitioning response to climate perturbations is generally additive and scalable (Figure 4). This is unexpected, given the nonlinearity of the loss functions and time series responses shown in Figure 1, but may prove quite useful in both parameterized land surface schemes in global climate models and in estimating climate impacts from the output of GCMs with simplified land surface hydrology representations. As an example, locally-estimated climate sensitivities for E_o, $\bar{P}$, and P_{X90} to surface temperature changes from a coupled model could be multiplied by the perturbation responses in Figure 2b-d for temperature-driven future scenario estimation of water flux partitioning.

There are, however, many processes that could change this linearity, including land-cover change, changes to seasonal water storage (snowpack), and land-atmosphere feedbacks such as convective triggering and changes in vegetation-controlled surface conductance and water-use efficiency. We hypothesize that the major non-linearities occur around the transition from water-limited to energy-limited states; thus, this simple additivity is unlikely to hold for shifts large enough to transition between moisture regimes (see the Central Plains, Supplementary Figure 8).

Our method for amplifying precipitation extremes is simple, and one of many possible approaches to represent this process. Actually characterizing the local changes to the precipitation distribution as a function of global mean temperature changes is likely empirically intractable, due to the magnitude of internal variability relative to low-frequency signals (Gianotti et al., 2014). Similarly, we do not investigate changes in the timing of precipitation (Pal et al., 2013) or storm/interstorm durations, which might expose more of the nonlinearity of the land surface flux partitioning. The results of these investigations would only be as robust as our estimation of the climate signal itself, which remains highly uncertain at this time.

While the superposability and scaling of impacts of climate perturbations is similar to the assumptions of aridity-index based hydroclimatology frameworks (Budyko), we find differences between these frameworks and our observation-driven scheme. These differences include large biases in changes to evaporation and drainage when precipitation extremes change (Figure 4). This suggests that mean-state conditions alone (E_o, seasonal P totals) are not sufficient to

characterize changes to land-surface wetting of the atmosphere and surface- and ground-water resource supplies under changing climate scenarios.

Two major consequences of using our more process-based representation over a steady-state aridity-index formulation are 1) that transient changes in water storage (not part of the Budyko scheme) are significant for global change scenarios which display trends/shifts in surface moisture regimes, and 2) that assumptions embedded in aridity-index frameworks where E/D partitioning responds identically to a 10% increase in seasonal precipitation as to a 10% decrease in E_o neglect the significant nuance of water balance dynamics. We argue that both of these effects are important, and that the dynamic system state of (2) — summarized here as the probability distribution of soil moisture — plays a role in the long-term average E and D partitioning. This is shown clearly in the P_{X90} experiment in Figures 2d, 4c, and 5c,f.

GCM studies suggest trends towards drier warm season surface soils, but perhaps wetter subsurface soils (Berg et al., 2017), which align with our global mean-state perturbation experiments (Figure 2e and Supplementary Figure 2). We argue that this is the expected consequence of an increase in both water supply and water demand, and that these trends are likely to only be amplified by increases in precipitation extremes (heavy days and dry spells).

The results of this study suggest that caution is necessary when viewing land surface conditions through a simple aridity lens when asking questions about global change. The downstream responses to water supply and demand will depend on the dynamics and distribution of land surface state variables (e.g., soil moisture). Changes in these state variables will more directly determine how the continental water cycle responds to global climate change.

References

Akbar, R., Short Gianotti, D. J., McColl, K. A., Haghighi, E., Salvucci, G. D., & Entekhabi, D. (2018). Estimation of landscape soil water losses from satellite observations of soil moisture. *Journal of Hydrometeorology*, *19*(5), 871–889. https://doi.org/10.1175/JHM-D-17-0200.1

Akbar, R., Short Gianotti, D. J., Salvucci, G. D., & Entekhabi, D. (2019). Mapped Hydroclimatology of Evapotranspiration and Drainage Runoff Using SMAP Brightness

372 Temperature Observations and Precipitation Information. *Water Resources Research*, *55*,
373 3391–3413.

374 Anderson, B. T., Gianotti, D. J., & Salvucci, G. D. (2015). Detectability of historical trends in
375 station-based precipitation characteristics over the continental united states. *Journal of*
376 *Geophysical Research*, *120*(10), 4842–4859. https://doi.org/10.1002/2014JD022960

377 Andréassian, V., Coron, L., Lerat, J., & Le Moine, N. (2016). Climate elasticity of streamflow
378 revisited - An elasticity index based on long-term hydrometeorological records. *Hydrology*
379 *and Earth System Sciences*, *20*(11), 4503–4524. https://doi.org/10.5194/hess-20-4503-2016

380 Berg, A., & Sheffield, J. (2018). Climate Change and Drought: the Soil Moisture Perspective.
381 *Current Climate Change Reports*, *4*(2), 180–191. https://doi.org/10.1007/s40641-018-0095-
382 0

383 Berg, A., Findell, K., Lintner, B., Giannini, A., Seneviratne, S. I., van den Hurk, B., et al. (2016).
384 Land–atmosphere feedbacks amplify aridity increase over land under global warming.
385 *Nature Climate Change*, *6*(May). https://doi.org/10.1038/nclimate3029

386 Berg, A., Sheffield, J., & Milly, P. C. D. (2017). Divergent surface and total soil moisture
387 projections under global warming. *Geophysical Research Letters*, *44*, 236–244.
388 https://doi.org/10.1002/2016GL071921

389 Berghuijs, W. R., Larsen, J. R., van Emmerik, T. H. M., & Woods, R. A. (2017). A Global
390 Assessment of Runoff Sensitivity to Changes in Precipitation, Potential Evaporation, and
391 Other Factors. *Water Resources Research*, *53*(10), 8475–8486.
392 https://doi.org/10.1002/2017WR021593

393 Budyko, M. I. (1963). *Evaporation under natural conditions*. Isreal Program for Scientific
394 Translations.

395 Byrne, M. P., & O'Gorman, P. A. (2015). The response of precipitation minus
396 evapotranspiration to climate warming: Why the "Wet-get-wetter, dry-get-drier" scaling
397 does not hold over land. *Journal of Climate*, *28*(20), 8078–8092.
398 https://doi.org/10.1175/JCLI-D-15-0369.1

399 Chen, M., Shi, W., Xie, P., Silva, V. B. S., Kousky, V. E., Higgins, R. W., & Janowiak, J. E.
400 (2008). Assessing objective techniques for gauge-based analyses of global daily
401 precipitation. *Journal of Geophysical Research Atmospheres*, *113*(4), 1–13.
402 https://doi.org/10.1029/2007JD009132

403 Chiew, F. H. S. (2006). Estimation of rainfall elasticity of streamflow in Australia. *Hydrological*
404 *Sciences Journal*, *51*(4), 613–625. https://doi.org/10.1623/hysj.51.4.613

405 Choudhury, B. J. (1999). Evaluation of an empirical equation for annual evaporation using field
406 observations and results from a biophysical model. *Journal of Hydrology*, *216*(1–2), 99–
407 110. https://doi.org/10.1016/S0022-1694(98)00293-5

408 Clapp, R. B., & Hornberger, G. M. (1978). Empirical Equations for Some Soil Hydraulic
409 Properties. *Water Resources Research*, *14*(4), 601–604.

410 Dai, A., Zhao, T., & Chen, J. (2018). Climate Change and Drought: a Precipitation and
411 Evaporation Perspective. *Current Climate Change Reports*, *4*(3), 301–312.
412 https://doi.org/10.1007/s40641-018-0101-6

413 Entekhabi, D., Njoku, E. G., O'Neill, P. E., Kellogg, K. H., Crow, W. T., Edelstein, W. N., et al.
414 (2010). The Soil Moisture Active Passive (SMAP) Mission. *Proceedings of the IEEE*,
415 *98*(5), 704–716. https://doi.org/10.1109/JPROC.2010.2043918

416 Fläschner, D., Mauritsen, T., & Stevens, B. (2016). Understanding the intermodel spread in
417 global-mean hydrological sensitivity. *Journal of Climate*, *29*(2), 801–817.
418 https://doi.org/10.1175/JCLI-D-15-0351.1

419 Fu, G., Charles, S. P., & Chiew, F. H. S. (2007). A two-parameter climate elasticity of
420 streamflow index to assess climate change effects on annual streamflow. *Water Resources*
421 *Research*, *43*(11), W11419. https://doi.org/10.1029/2007WR005890

422 Fu, Q., & Feng, S. (2014). Responses of terrestrial aridity to global warming. *Journal of*
423 *Geophysical Research: Atmospheres*, (119), 7863–7875.
424 https://doi.org/10.1002/2014JD021608

Gianotti, D. J. S., Anderson, B. T., & Salvucci, G. D. (2014). The potential predictability of precipitation occurrence, intensity, and seasonal totals over the continental United States. *Journal of Climate*, *27*(18), 6904–6918. https://doi.org/10.1175/JCLI-D-13-00695.1

Greve, P., & Seneviratne, S. I. (2015). Assessment of future changes in water availability and aridity. *Geophysical Research Letters*, *42*(13), 5493–5499. https://doi.org/10.1002/2015GL064127

Greve, P., Orlowsky, B., Mueller, B., Sheffield, J., Reichstein, M., & Seneviratne, S. I. (2014). Global assessment of trends in wetting and drying over land. *Nature Geoscience*, *7*(10), 716–721. https://doi.org/10.1038/NGEO2247

Greve, P., Gudmundsson, L., & Seneviratne, S. I. (2018). Regional scaling of annual mean precipitation and water availability with global temperature change. *Earth System Dynamics*, *9*(1), 227–240. https://doi.org/10.5194/esd-9-227-2018

Gu, X., Zhang, Q., Li, J., Singh, V. P., Liu, J., Sun, P., & Cheng, C. (2019). Attribution of Global Soil Moisture Drying to Human Activities: A Quantitative Viewpoint. *Geophysical Research Letters*, 1–10. https://doi.org/10.1029/2018GL080768

Haghighi, E., Short Gianotti, D. J., Akbar, R., Salvucci, G. D., & Entekhabi, D. (2018). Soil and Atmospheric Controls on the Land Surface Energy Balance: A Generalized Framework for Distinguishing Moisture- and Energy-Limited Evaporation Regimes. *Water Resources Research*, 1–21. https://doi.org/10.1002/2017WR021729

Hartmann, D. L., Tank, A. M. G. K., M. Rusticucci, L. V., Alexander, S. B., Charabi, Y., Dentener, F. J., et al. (2013). *Observations: Atmosphere and Surface*. *Climate Change 2013 the Physical Science Basis: Working Group I Contribution to the Fifth Assessment Report of the Intergovernmental Panel on Climate Change* (Vol. 9781107057). Cambridge, UK and New York, NY, USA: Cambridge University Press. https://doi.org/10.1017/CBO9781107415324.008

Hawkins, E., & Sutton, R. (2011). The potential to narrow uncertainty in projections of regional precipitation change. *Climate Dynamics*, *37*(1), 407–418. https://doi.org/10.1007/s00382-

010-0810-6

Hirabayashi, Y., Mahendran, R., Koirala, S., Konoshima, L., Yamazaki, D., Watanabe, S., et al. (2013). Global flood risk under climate change. *Nature Climate Change*, *3*(9), 816–821. https://doi.org/10.1038/nclimate1911

Kharin, V. V., Zwiers, F. W., Zhang, X., & Wehner, M. (2013). Changes in temperature and precipitation extremes in the CMIP5 ensemble. *Climatic Change*, *119*(2), 345–357. https://doi.org/10.1007/s10584-013-0705-8

Koster, R. D., Guo, Z., Yang, R., Dirmeyer, P. A., Mitchell, K., & Puma, M. J. (2009). On the nature of soil moisture in land surface models. *Journal of Climate*, *22*(16), 4322–4335. https://doi.org/10.1175/2009JCLI2832.1

Koster, R. D., Crow, W. T., Reichle, R. H., & Mahanama, S. P. (2018). Estimating Basin-Scale Water Budgets With SMAP Soil Moisture Data. *Water Resources Research*, *54*(7), 4228–4244. https://doi.org/10.1029/2018WR022669

Lambert, F. H., & Webb, M. J. (2008). Dependency of global mean precipitation on surface temperature. *Geophysical Research Letters*, *35*(16), 1–5. https://doi.org/10.1029/2008GL034838

McVicar, T. R., Roderick, M. L., Donohue, R. J., Li, L. T., Van Niel, T. G., Thomas, A., et al. (2012). Global review and synthesis of trends in observed terrestrial near-surface wind speeds: Implications for evaporation. *Journal of Hydrology*, *416*, 182–205. https://doi.org/10.1016/j.jhydrol.2011.10.024

Milly, P. C. D., & Dunne, K. A. (2016). Potential evapotranspiration and continental drying. *Nature Climate Change*, *6*, 946-951``. https://doi.org/10.1038/NCLIMATE3046

Muller, C. J., O'Gorman, P. A., & Back, L. E. (2011). Intensification of precipitation extremes with warming in a cloud-resolving model. *Journal of Climate*, *24*(11), 2784–2800. https://doi.org/10.1175/2011JCLI3876.1

Novick, K. A., Ficklin, D. L., Stoy, P. C., Williams, C. A., Bohrer, G., Oishi, A. C., et al. (2016).

The increasing importance of atmospheric demand for ecosystem water and carbon fluxes. *Nature Climate Change*, *1*(September), 1–5. https://doi.org/10.1038/nclimate3114

O'Gorman, P. A., & Schneider, T. (2008). The hydrological cycle over a wide range of climates simulated with an idealized GCM. *Journal of Climate*, *21*(15), 3815–3832. https://doi.org/10.1175/2007JCLI2065.1

O'Gorman, P. A., & Schneider, T. (2009). The physical basis for increases in precipitation extremes in simulations of 21st-century climate change. *Proceedings of the National Academy of Sciences of the United States of America*, *106*(35), 14773–14777. https://doi.org/10.1073/pnas.0907610106

O'Gorman, P. A., Allan, R. P., Byrne, M. P., & Previdi, M. (2012). Energetic Constraints on Precipitation Under Climate Change. *Surveys in Geophysics*, *33*(3–4), 585–608. https://doi.org/10.1007/s10712-011-9159-6

O'Neill, P. E., Chan, S., Njoku, E. G., Jackson, T., & Bindlish, R. (2016). SMAP L3 Radiometer Global Daily 36 km EASE-Grid Soil Moisture, Version 4. Boulder, Colorado USA: NASA National Snow and Ice Data Center Distributed Active Archive Center. https://doi.org/10.5067/OBBHQ5W22HME

Oldekop, E. (1911). *Evaporation from the surface of river basins (Испареніе съ поверхности речныхъ бассейновъ)*. University of Tartu-Jurjew-Dorpat, Tartu, Estonia.

Pal, I., Anderson, B. T., Salvucci, G. D., & Gianotti, D. J. (2013). Shifting seasonality and increasing frequency of precipitation in wet and dry seasons across the U.S. *Geophysical Research Letters*, *40*(15), 4030–4035. https://doi.org/10.1002/grl.50760

Pall, P., Allen, M. R., & Stone, D. A. (2007). Testing the Clausius-Clapeyron constraint on changes in extreme precipitation under CO2 warming. *Climate Dynamics*, *28*(4), 351–363. https://doi.org/10.1007/s00382-006-0180-2

Pendergrass, A. G., Knutti, R., Lehner, F., Deser, C., & Sanderson, B. M. (2017). Precipitation variability increases in a warmer climate. *Scientific Reports*, *7*(1), 1–9. https://doi.org/10.1038/s41598-017-17966-y

505 Prein, A. F., & Pendergrass, A. G. (2019). Can we Constrain Uncertainty in Hydrologic Cycle
506 Projections? *Geophysical Research Letters*, (2018), 2018GL081529.
507 https://doi.org/10.1029/2018GL081529

508 Rigden, A. J., Salvucci, G. D., Entekhabi, D., & Short Gianotti, D. J. (2018). Partitioning
509 Evapotranspiration Over the Continental United States Using Weather Station Data.
510 *Geophysical Research Letters*, *45*(18), 9605–9613. https://doi.org/10.1029/2018GL079121

511 Risbey, J. S., & Entekhabi, D. (1996). Observed Sacramento Basin streamflow response to
512 precipitation and temperature changes and its relevance to climate impact studies. *Journal*
513 *of Hydrology*, *184*(3–4), 209–223. https://doi.org/10.1016/0022-1694(95)02984-2

514 Roderick, M. L., & Farquhar, G. D. (2011). A simple framework for relating variations in runoff
515 to variations in climatic conditions and catchment properties. *Water Resources Research*,
516 *47*(6), 1–11. https://doi.org/10.1029/2010WR009826

517 Roderick, M. L., Sun, F., Lim, W. H., & Farquhar, G. D. (2014). A general framework for
518 understanding the response of the water cycle to global warming over land and ocean.
519 *Hydrology and Earth System Sciences*, *18*(5), 1575–1589. https://doi.org/10.5194/hess-18-
520 1575-2014

521 Romps, D. M. (2011). Response of Tropical Precipitation to Global Warming. *Journal of the*
522 *Atmospheric Sciences*, *68*(1), 123–138. https://doi.org/10.1175/2010jas3542.1

523 Samset, B. H., Myhre, G., Forster, P. M., Hodnebrog, Andrews, T., Faluvegi, G., et al. (2016).
524 Fast and slow precipitation responses to individual climate forcers: A PDRMIP multimodel
525 study. *Geophysical Research Letters*, *43*(6), 2782–2791.
526 https://doi.org/10.1002/2016GL068064

527 Sankarasubramanian, A., Vogel, R. M., & Limbrunner, J. F. (2001). Climate elasticity of
528 streamflow in the United States. *Water Resources Research*, *37*(6), 1771–1781.
529 https://doi.org/10.1029/2000WR900330

530 Scheff, J., & Frierson, D. M. W. (2014). Scaling potential evapotranspiration with greenhouse
531 warming. *Journal of Climate*, *27*(4), 1539–1558. https://doi.org/10.1175/JCLI-D-13-

00233.1

Schewe, J., Heinke, J., Gerten, D., Haddeland, I., Arnell, N. W., Clark, D. B., et al. (2014). Multimodel assessment of water scarcity under climate change. *Proceedings of the National Academy of Sciences*, *111*(9), 3245–3250. https://doi.org/10.1073/pnas.1222460110

Short Gianotti, D. J., Rigden, A. J., Salvucci, G. D., & Entekhabi, D. (2019). Satellite and Station Observations Demonstrate Water Availability's Effect on Continental-Scale Evaporative and Photosynthetic Land Surface Dynamics. *Water Resources Research*, *55*(1), 540–554. https://doi.org/10.1029/2018WR023726

Sohn, B. J., & Park, S. C. (2010). Strengthened tropical circulations in past three decades inferred from water vapor transport. *Journal of Geophysical Research Atmospheres*, *115*(15), 1–9. https://doi.org/10.1029/2009JD013713

Swann, A. L. S. (2018). Plants and Drought in a Changing Climate. *Current Climate Change Reports*, *4*(2), 192–201. https://doi.org/10.1007/s40641-018-0097-y

Thackeray, C. W., DeAngelis, A. M., Hall, A., Swain, D. L., & Qu, X. (2018). On the Connection Between Global Hydrologic Sensitivity and Regional Wet Extremes. *Geophysical Research Letters*, *45*(20), 11,343-11,351. https://doi.org/10.1029/2018GL079698

Turc, L. (1954). The water balance of soils: relationship between precipitations, evaporation and flow (Le bilan d'eau des sols: relation entre les précipitations, l'évaporation et l'écoulement). *Annales Agronomiques, Série A*, *5*, 491–595.

Vecchi, G. A., Soden, B. J., Wittenberg, A. T., Held, I. M., Leetmaa, A., & Harrison, M. J. (2006). Weakening of tropical Pacific atmospheric circulation due to anthropogenic forcing. *Nature*, *441*(1), 73–76. https://doi.org/10.1038/nature04744

Yang, H., & Yang, D. (2011). Derivation of climate elasticity of runoff to assess the effects of climate change on annual runoff. *Water Resources Research*, *47*(7), 1–12. https://doi.org/10.1029/2010WR009287

Acknowledgements

Soil moisture (SMAP) data are available from the National Snow and Ice Data Center portal (http://www.nsidc.org). Precipitation data are available from the NCEP ftp portal (ftp.cpc.ncep.noaa.gov/precip/CPC_UNI_PRCP/) The authors acknowledge no conflicts of interest.

565

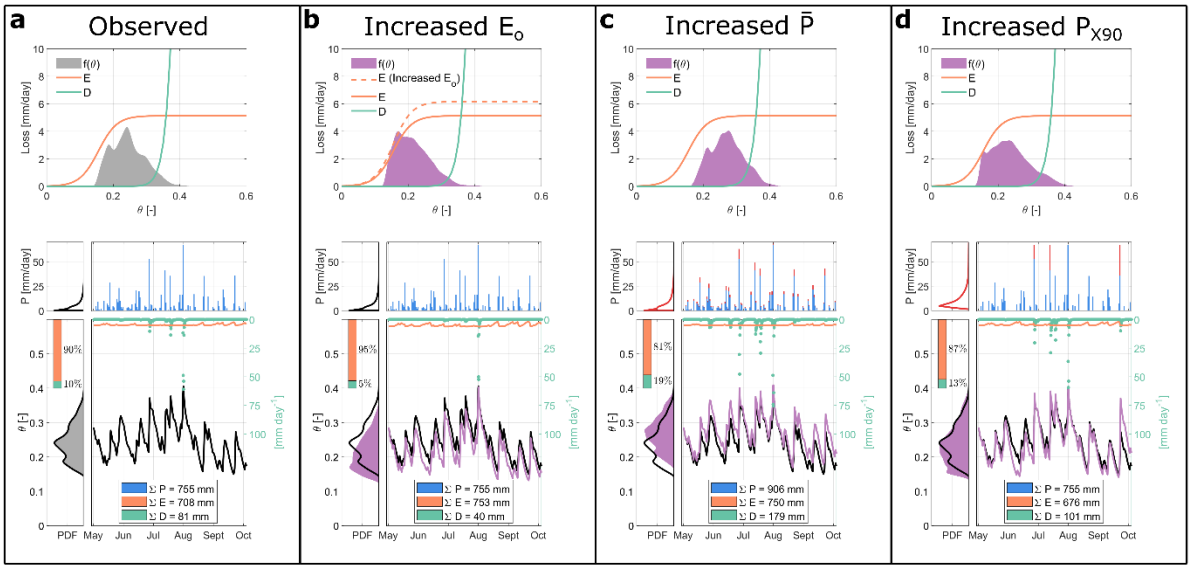

Figure 1: Example evaporation and drainage loss losses for observations and experimental perturbations for a location in Southern Iowa, summer 2015. a) Retrieved evaporation (E) and drainage (D) loss functions; observed precipitation (P); and time series of soil moisture (θ), E, and D based on observations. Grey shaded regions show the marginal probability density (PDF) of soil moisture $f(\theta)$. Blue bars show daily precipitation with accompanying PDF for wet days. Black line, orange line, and green markers show θ, E, and D time series (E and D shown on right axis). Orange (green) bar shows E's (D's) fractional contribution to seasonal outfluxes from the land surface. b) Same as (a), except for the increased potential evaporation (E_o) experiment using the orange dashed line for $E(\theta)$. Precipitation unchanged, but $f(\theta)$ moves towards drier conditions where E losses dominate D. c) Same as (a) except for with increased daily precipitation, shown as red bars above observed (blue) precipitation bars. $f(\theta)$ (in red) shifts to wetter conditions, increasing D. d) Same as (a) except with increased precipitation extremes (mean and maximum daily P unchanged). Red P bars show added precipitation on wet days, taken from an equal amount of precipitation removed on drier days. $f(\theta)$ (in red) increases the wet tail at the expense of the dry tail, leading to increased D 0.and reduced E.

585

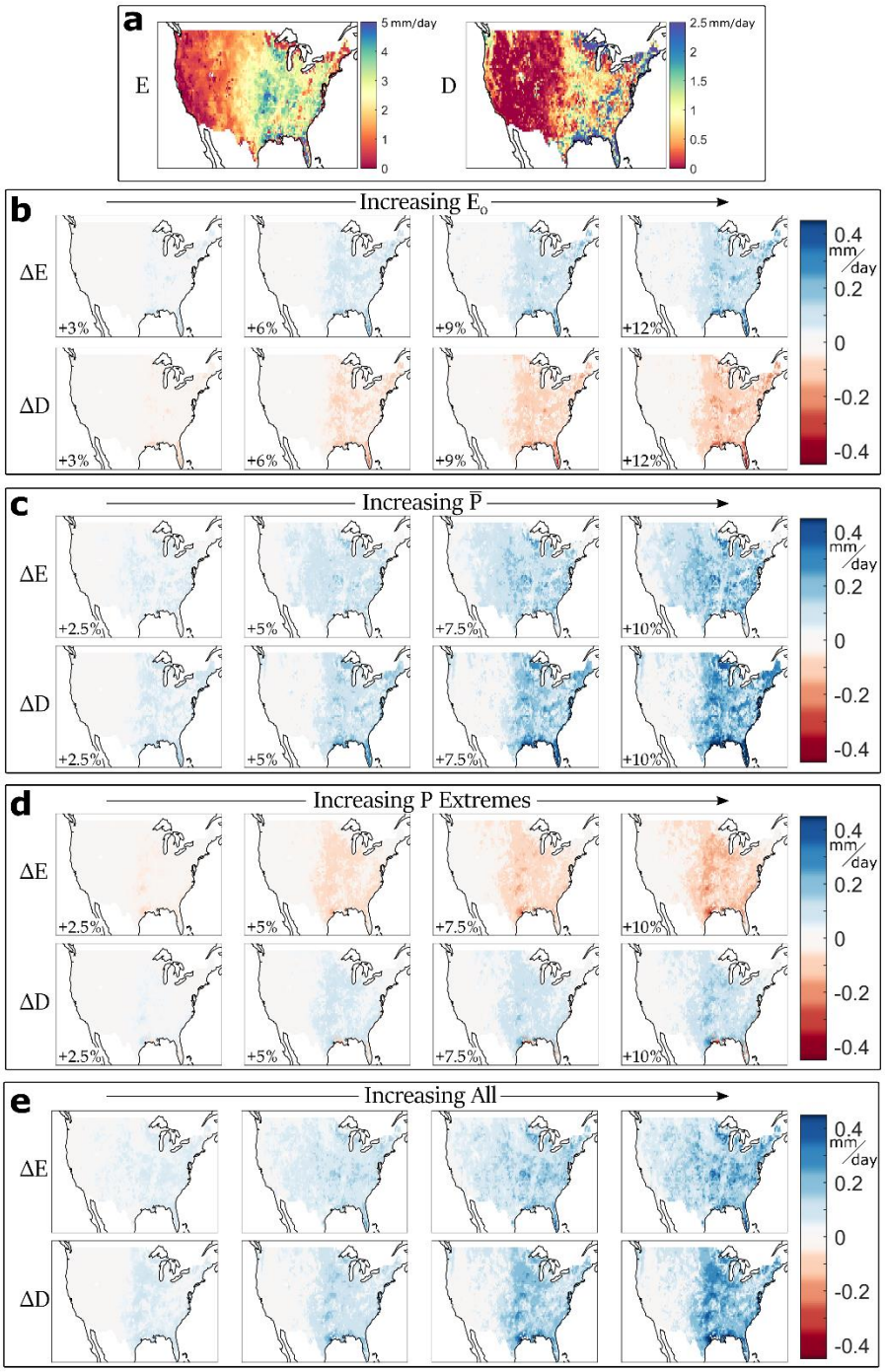

586

587 **Figure 2: Evaporation, drainage, and hydrologic sensitivities to climate perturbations.** a)
588 Mean evaporation (E) and drainage (D) for warm season 2015–2017 from the estimated loss
589 functions and climate perturbations. b) First column shows changes ΔE and ΔD relative to (a) for

a 3% increase in E_o. Columns 2–4 show impacts for E_o increases of 6%, 9%, and 12%. Evaporation increases across the ConUS and drainage decreases, with the most substantial changes in the energy-limited East. c) Same as (b) but for perturbations to $\bar{P}$. d) Same as (b) but for increases in extreme precipitation (percentages show heaviest decile increase — no change in $\bar{P}$). e) Changes in mean E and D when simultaneously combining the impacts of increased E_o, $\bar{P}$, and precipitation extremes.

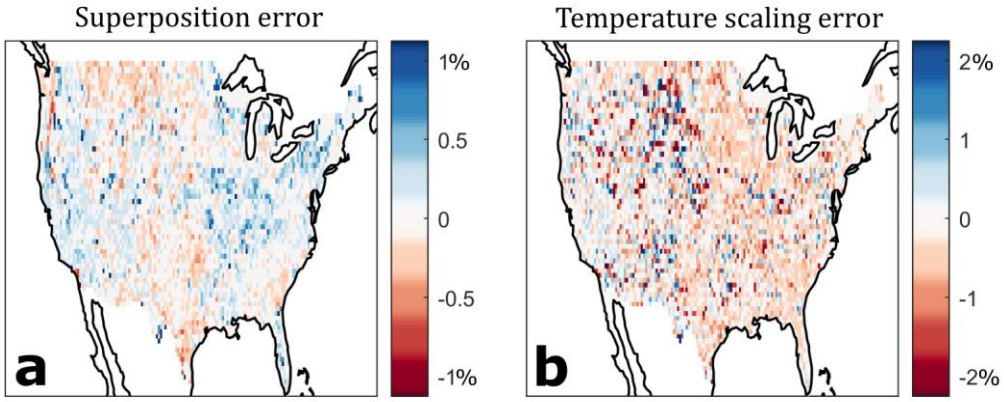

Figure 3: Superposability and scaling of individual perturbations. a) The percentage error in evaporation when adding the individual E_o, mean P, and extreme P perturbations (the sum of the rightmost column of Figure 2b-d) in place of the fully-coupled system (rightmost column of Figure 2e). b) The percentage error in evaporation when assuming linear temperature-equivalent scaling of perturbations (4 times the leftmost column of Figure 2e in place of the rightmost column of Figure 2e). Both the superposition errors and the scaling errors are small (~1-2%), suggesting that the effects shown in Figure 2b-d can be combined and scaled directly based on local estimated climate sensitivities of E_o, $\bar{P}$, and P extremes. See also Supplementary Figures 8-9.

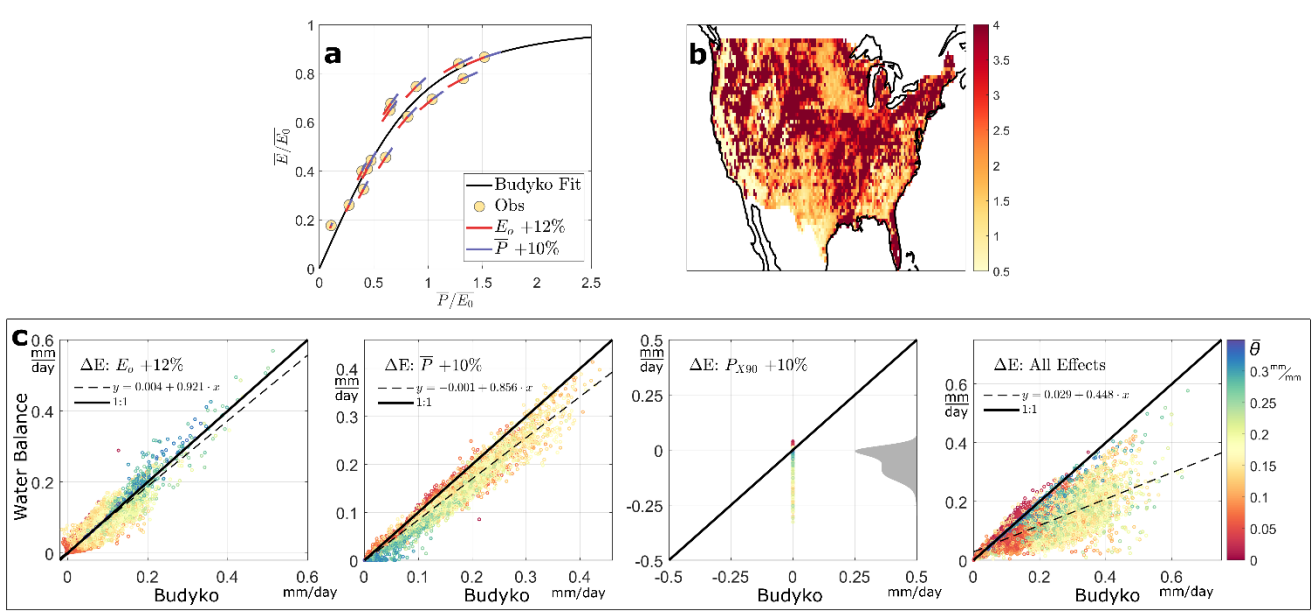

Figure 4: Comparison with Budyko hydroclimatological framework. a) The classical Budyko curve fit to a single location. Each point is a month of mean evaporation $\bar{E}$ versus mean precipitation $\bar{P}$, both normalized by potential evaporation E_o. Evaporation time series and estimated potential evaporation are from the integration of the water balance (1)-(3). Lines show the shift in $\bar{E}/E_o$ that follows a change in $\bar{P}/E_o$ by changing E_o (red) or $\bar{P}$ (blue). Equal E_o and $\bar{P}$ changes cancel each other. b) The estimated Budyko n parameter for each location: $\bar{E} = \bar{P} \cdot E_o \cdot (\bar{P}^n + E_o^n)^{-\frac{1}{n}}$. c) Comparison of changes in evaporation ΔE versus the Budyko method. Plots show comparison for increased E_o, increased $\bar{P}$, increased precipitation extremes (P_{X90}), and all simultaneous effects combined. Colors show mean soil moisture calculated as part of the water balance. Bias in increased $\bar{P}$ comparison due primarily to changes in soil water storage. Bias in All Effects comparison due primarily to impact of precipitation extremes.

Figure 1.

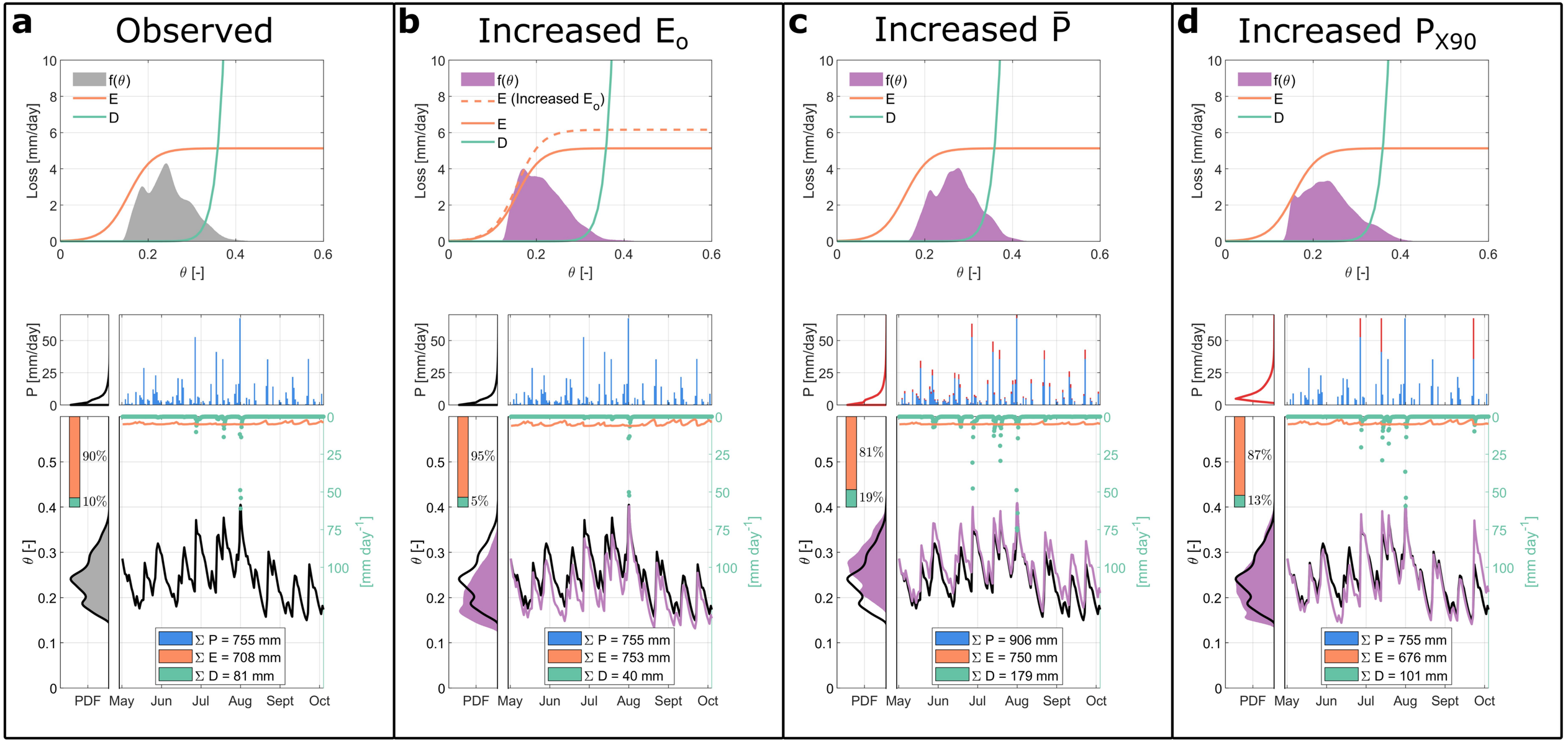
a
Observed
b
Increased E_o
c
Increased $\bar{P}$
d
Increased P_{X90}
f(θ)
E
D
E (Increased E_o)
Loss [mm/day]
θ [-]
P [mm/day]
θ [-]
[mm day^{-1}]
90%
10%
95%
5%
81%
19%
87%
13%
PDF
May
Jun
Jul
Aug
Sept
Oct
Σ P = 755 mm
Σ E = 708 mm
Σ D = 81 mm
Σ P = 755 mm
Σ E = 753 mm
Σ D = 40 mm
Σ P = 906 mm
Σ E = 750 mm
Σ D = 179 mm
Σ P = 755 mm
Σ E = 676 mm
Σ D = 101 mm

Figure 2.

a

E

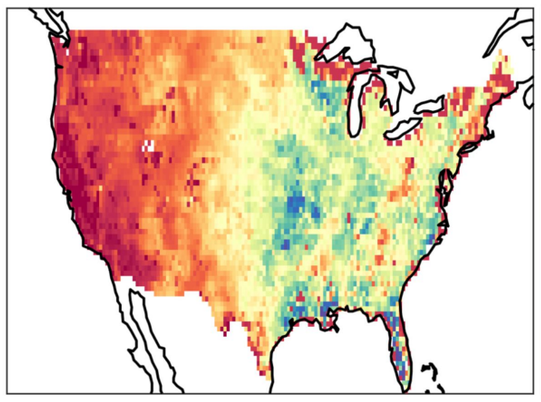

5 mm/day
4
3
2
1
0

D

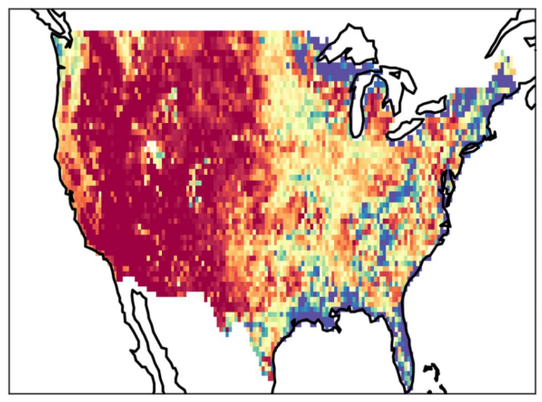

2.5 mm/day
2
1.5
1
0.5
0

b

Increasing E_o

ΔE

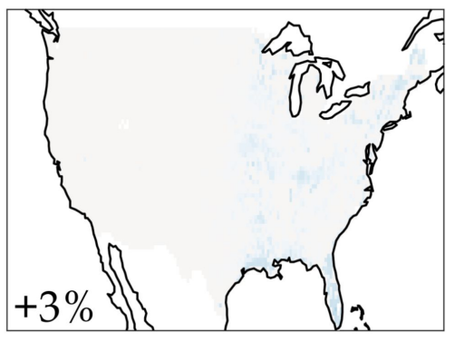

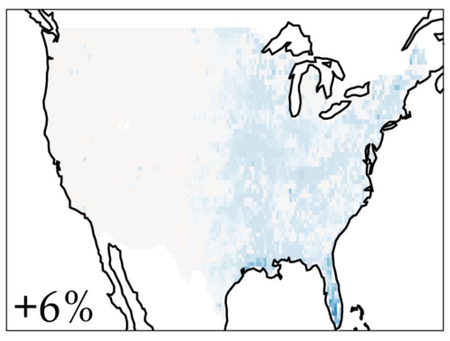

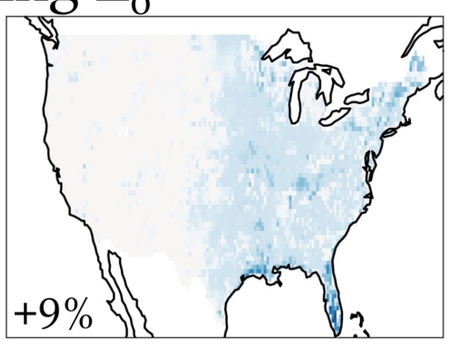

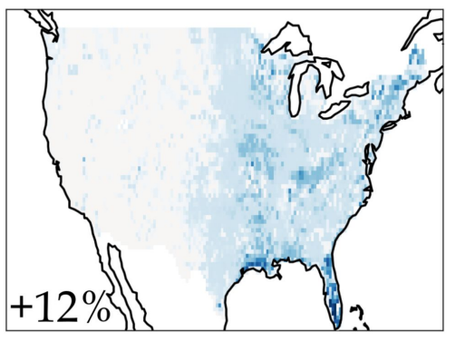

ΔD

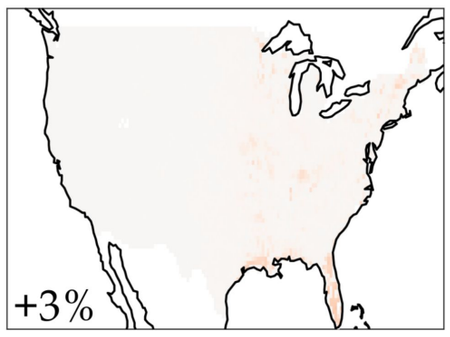

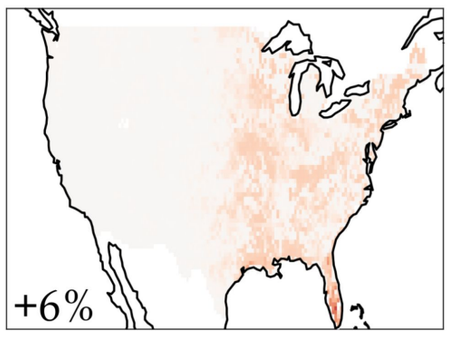

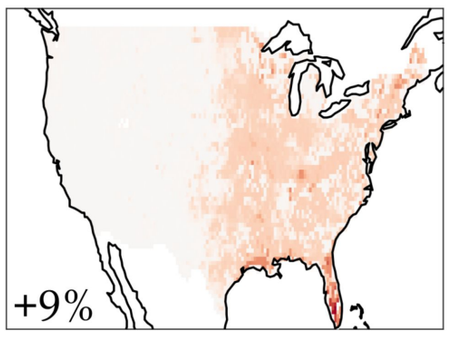

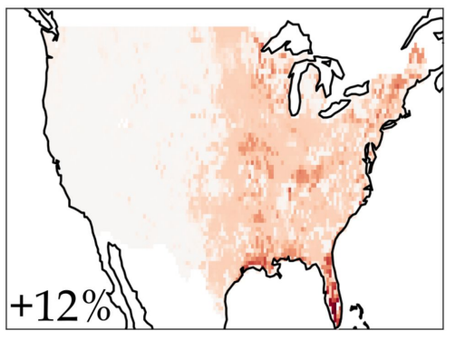

0.4
mm/day
0.2
0
-0.2
-0.4

c

Increasing $\bar{P}$

ΔE

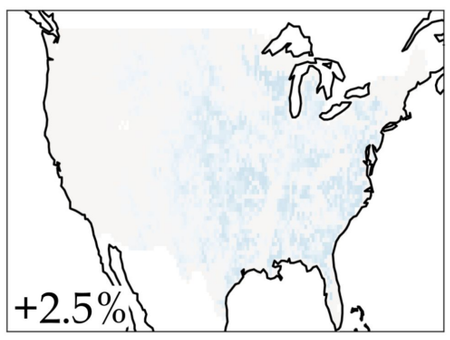

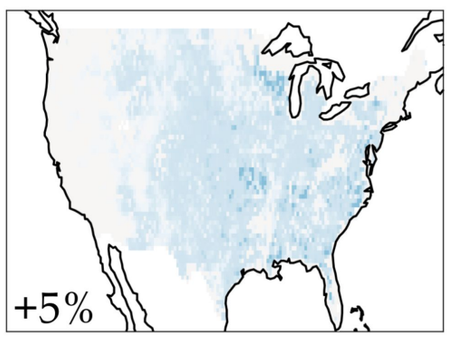

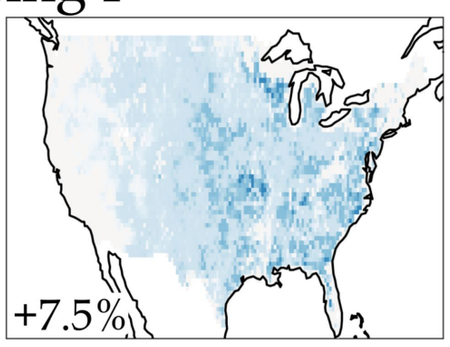

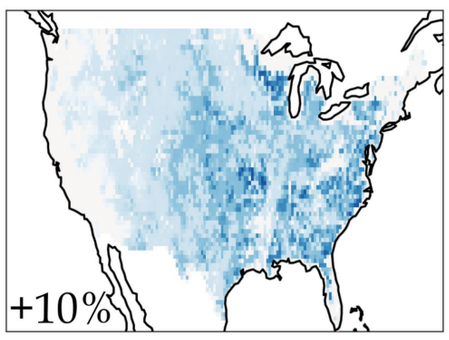

ΔD

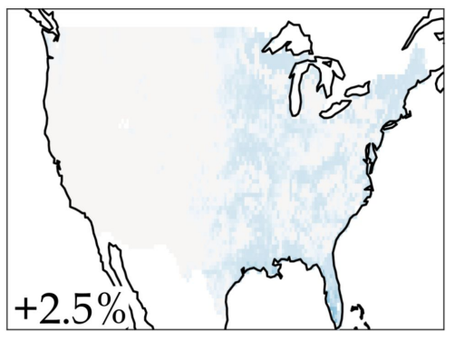

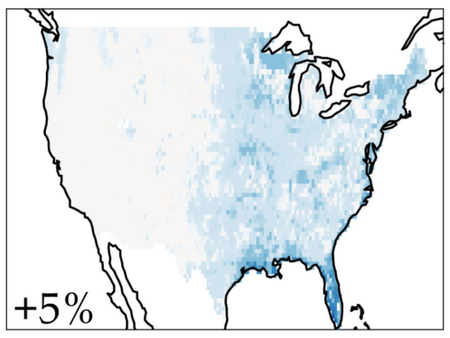

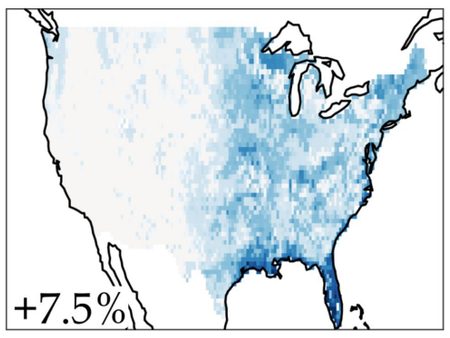

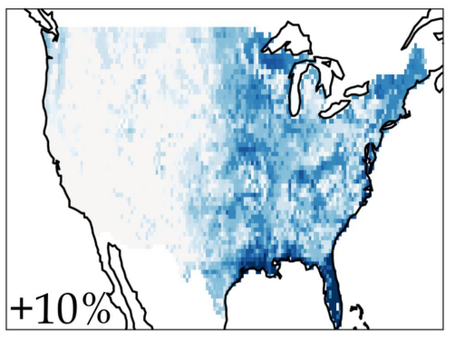

0.4
mm/day
0.2
0
-0.2
-0.4

d

Increasing P Extremes

ΔE

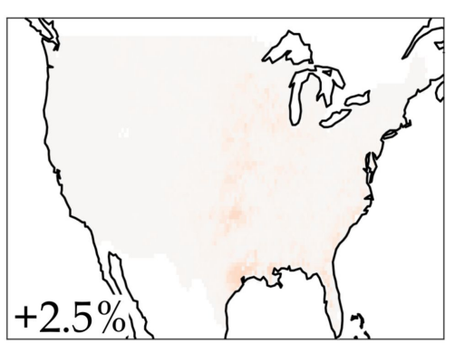

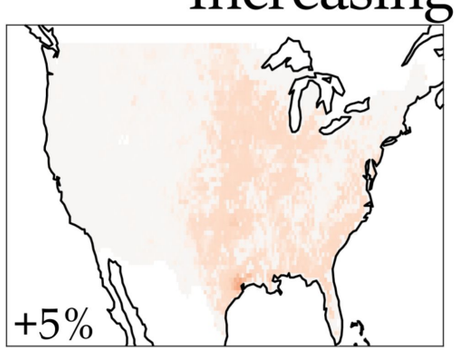

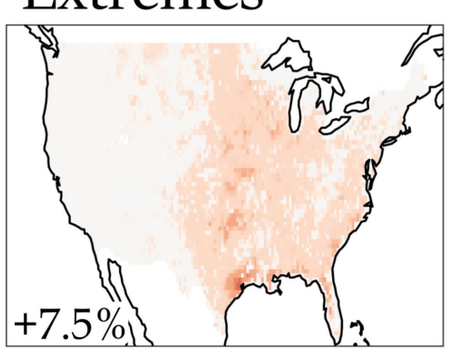

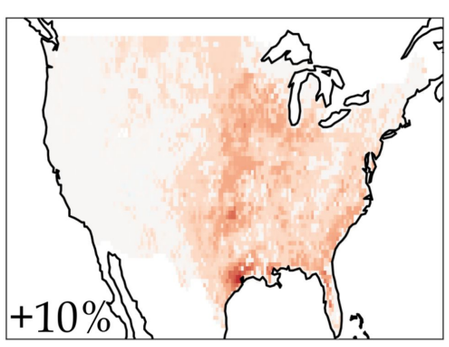

ΔD

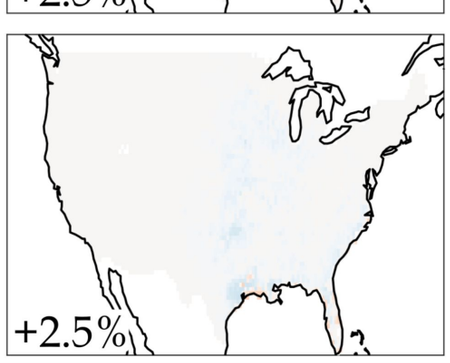

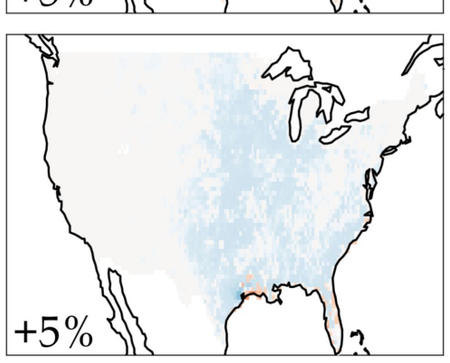

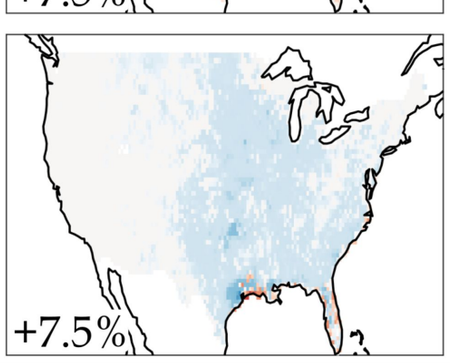

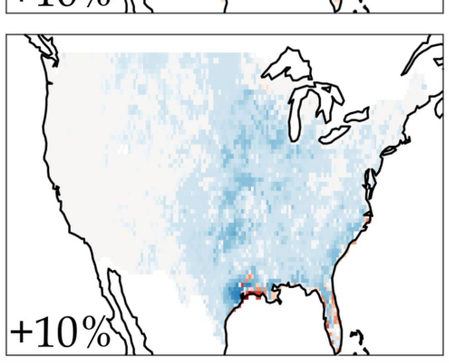

0.4
mm/day
0.2
0
-0.2
-0.4

e

Increasing All

ΔE

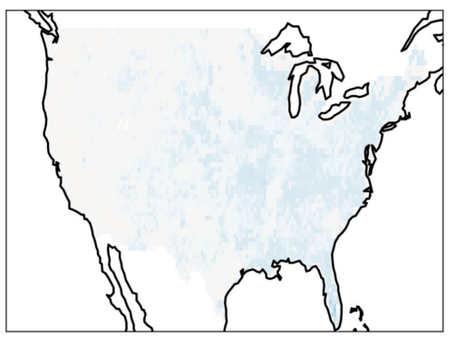

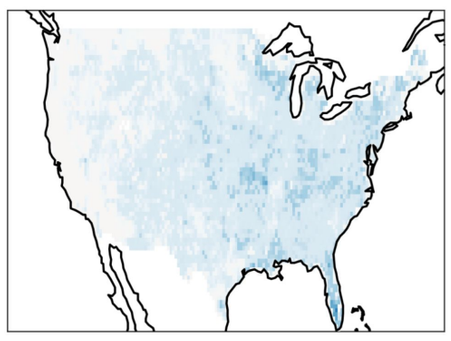

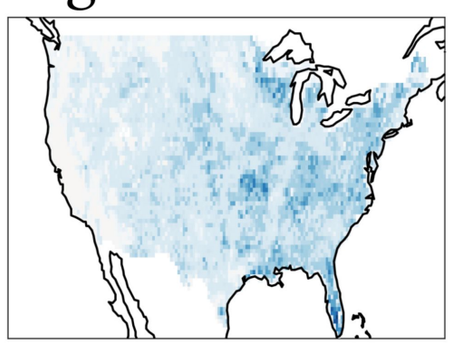

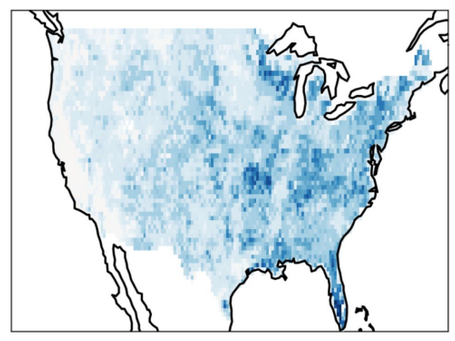

ΔD

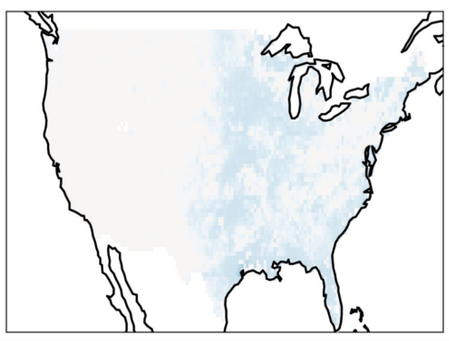

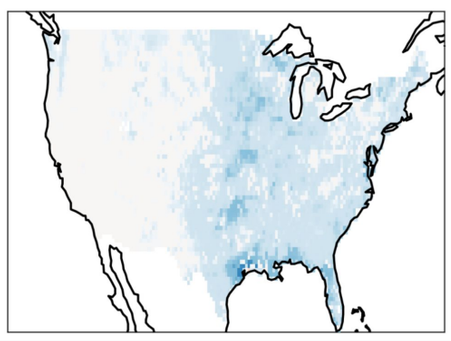

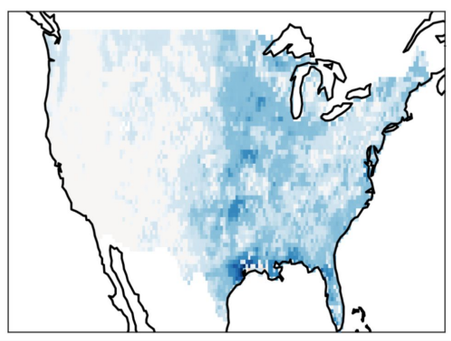

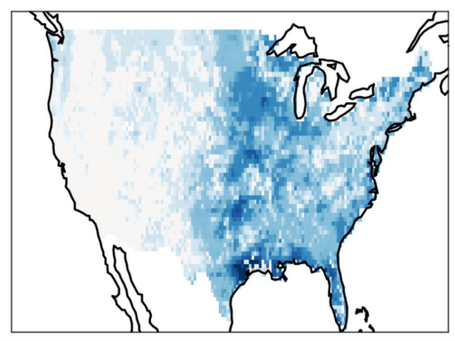

0.4
mm/day
0.2
0
-0.2
-0.4

Figure 3.

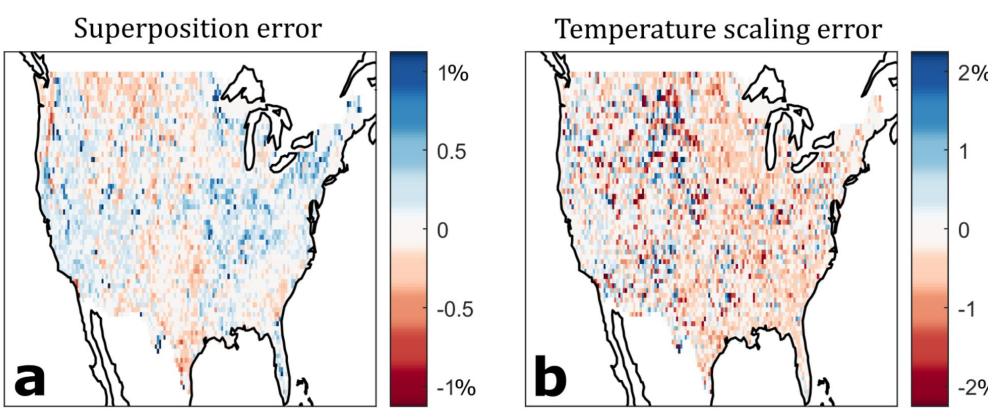
Superposition error
1%
0.5
0
-0.5
-1%
a
Temperature scaling error
2%
1
0
-1
-2%
b

Figure 4.

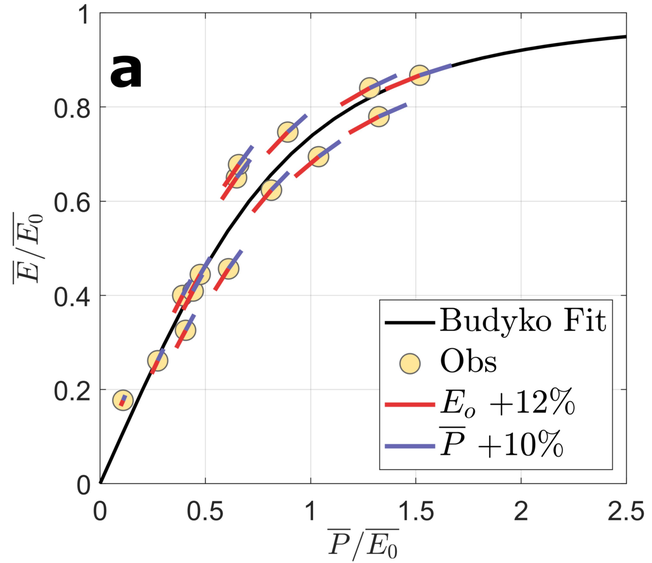
a
$\overline{E}/\overline{E_0}$
$\overline{P}/\overline{E_0}$
Budyko Fit
Obs
E_o +12%
$\overline{P}$ +10%

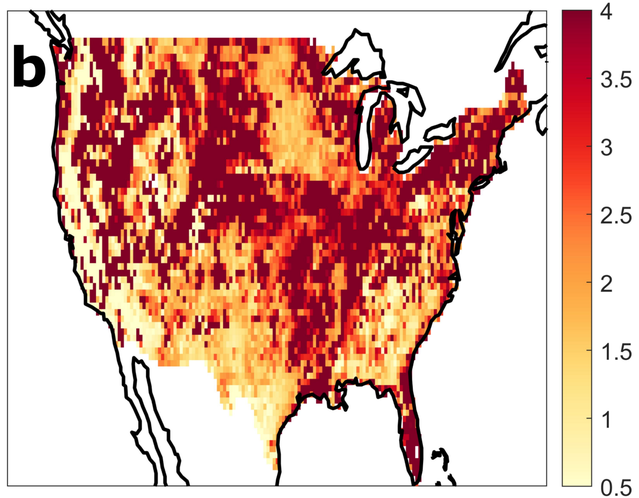
b

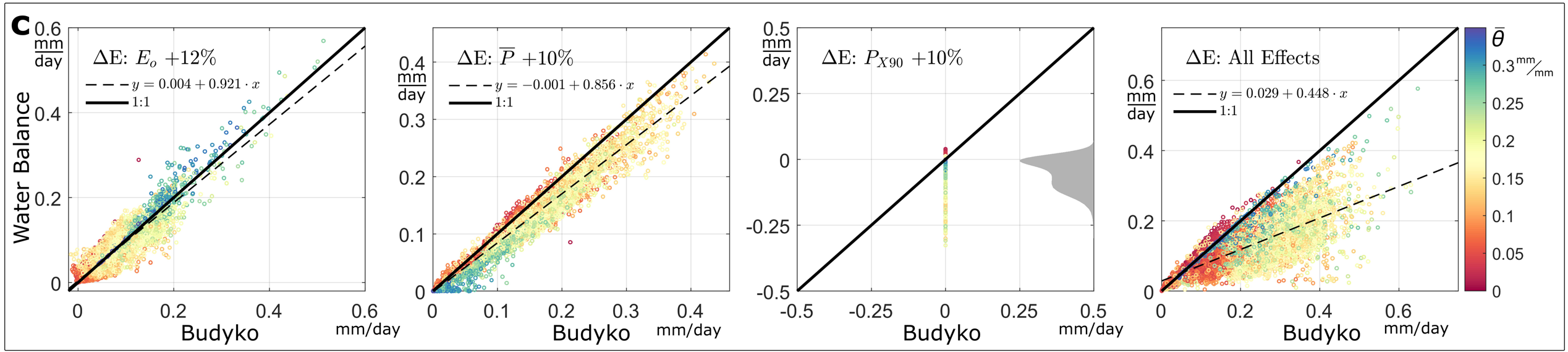
c
Water Balance
Budyko
mm/day
ΔE: E_o +12%
$y = 0.004 + 0.921 \cdot x$
1:1
ΔE: $\overline{P}$ +10%
$y = -0.001 + 0.856 \cdot x$
ΔE: P_{X90} +10%
ΔE: All Effects
$y = 0.029 + 0.448 \cdot x$
$\overline{\theta}$
mm/mm